



Preparation of black TiO₂ by hydrogen plasma assisted chemical vapor deposition and its photocatalytic activity



Feng Teng¹, Mingyang Li¹, Caitian Gao, Guozhi Zhang, Peng Zhang, Youqing Wang, Lulu Chen, Erqing Xie*

School of Physical Science and Technology, Lanzhou University, Lanzhou 730000, People's Republic of China

ARTICLE INFO

Article history:

Received 22 September 2013

Received in revised form 5 November 2013

Accepted 10 November 2013

Available online 15 November 2013

Keywords:

Black TiO₂

Hydrogen plasma

Disorder layer

Oxygen vacancy

Chromium ions

ABSTRACT

Black TiO₂ attracts enormous attention due to its large solar absorption and excellent photocatalytic activity. An approach assisted by hot filament hydrogen plasma to synthesize the black TiO₂ nanostructure is presented in our work. The black TiO₂ possesses a larger solar absorption, especially in the visible and near infrared region. The measurement results show that the oxygen vacancy and Ti–H are the major impacts to form disorder layer and the coloration of black. High absorption of light and numerous active sites ensure the excellent photocatalytic activity for the black TiO₂ in the photo-oxidation of organic molecules in water. Considered that Cr has important effect on the electronic structure of TiO₂ reported by some researchers, Cr ions were introduced into the structure of TiO₂, but Cr ions play the opposite role for its photocatalytic activity because it plays a role in the recombination of photo-generated carriers.

© 2013 Elsevier B.V. All rights reserved.

1. Introduction

With the development of the society, environmental issues become particularly important for the sustainable development of mankind. Elimination of environmental contaminants becomes an important task for all the scientists. Organic pollutants are the dominant contaminants, such as natural organic matters, industrial dyes, microorganisms and so on. Degradation by catalysts provides an attractive route to remove organic pollutants [1–3]. Semiconductor oxides are the optimal candidates because they can photo-degrade the organic dyes by absorbing light corresponding to the band gap. However, most photocatalysts can only be excited by ultraviolet (UV) light [4–6].

Searching for efficient semiconductors utilized visible-light to achieve the photocatalytic process remains a great challenge [7–10]. Owing to its narrower bandgap (< typical 3 eV value) enabling absorb visible light and relatively high electrical conductivity, defective TiO₂ is more attractive for photovoltaics, photocatalysis and fuel cells than bare TiO₂ [11–13]. Indeed, bandgap engineering is a crucial required technology to optimize TiO₂ solar light harvesting capability. And doping metal or nonmetal impurities are several interesting attempts [14–17].

However, the introduction of dopants, acting as charge carrier recombination centers, is a major impact to reduce the photocatalytic efficiency [18]. Recent studies performed on crystalline TiO₂ nanoparticles demonstrate that an enhanced solar absorption can be achieved through the introduction of disorder surface layers for nanophase TiO₂ through hydrogenation [19]. It was reported that exposure in hydrogen (H₂) led to a remarkable change in color, from white to black, when mid-band gap states are proposed to form. Since then, the synthesis of black titania has attracted plenty of attentions [20–27]. The typical preparation method is to anneal different titania precursors at about 500 °C under a H₂ flow. Many theoretical models were employed to explain the black coloration of titania, which include surface disorder, oxygen vacancy (Ti³⁺) [8,21,28], surface hydrogenation [29,30], even the material of the reaction vessel. Alon Danon et al. [31] reported that the prepared titanium oxide-based nanotubes changed color from white to black with a steel reactor at elevated temperatures and under the flow of hydrogen, when the same procedures were implemented in a quartz tube reactor, the color of the nanotubes changed to blue. They claimed that the presence of chromium (Cr) in the stainless steel reactor lead to the change in color from white to black. But considered Cr is unfriendly for environment, the influence of Cr needs further research. Generally speaking, many divergent interpretations still exist on the mechanism of the black titania production.

Herein, we report an approach assisted by hot filament hydrogen plasma to produce black titania nanostructure. This black

* Corresponding author. Tel.: +86 9318912616; fax: +86 9318913554.

E-mail address: xieeq@lzu.edu.cn (E. Xie).

¹ These authors contributed equally to this work.

titania nanostructure reveals strong visible and near infrared light absorption. We elucidate the inner workings of the black TiO_2 nanostructure are that abundant oxygen vacancies and Ti–H bonds are yielded to broaden the absorption region of visible light and provide numerous active sites for photo-degradation while Cr ions in the disorder layer play the opposite role.

2. Materials and methods

2.1. Preparation of black TiO_2

The titanium oxide nanostructures were prepared by a modification of previously reported hydrothermal method [32,33]. Briefly,

2 g of P25 powder (Degussa) was stirred for 10 min with 50 mL of sodium hydroxide (NaOH) solution (10 mol/L) in a 100 mL beaker. The obtained solution was transferred into a Teflon-lined stainless steel autoclave with an inner volume of 40 mL, and the autoclave has been sealed and placed in an oven before the oven was heated to 120 °C for 12 h. Then the resultant precipitate was washed with hydrochloric acid (HCl) solution (1 mol/L), followed by several washing using deionized water to attain a pH between 6 and 7. The prepared titania powder (TAN) was dried at 110 °C. The hydrogenation was performed in a hot-filament chemical vapor deposition (HFCVD) apparatus with hydrogen as reaction gas (as shown in Scheme S1, ESI) [34,35]. HFCVD is the most promising options to generate hydrogen plasma compared to other methods because its

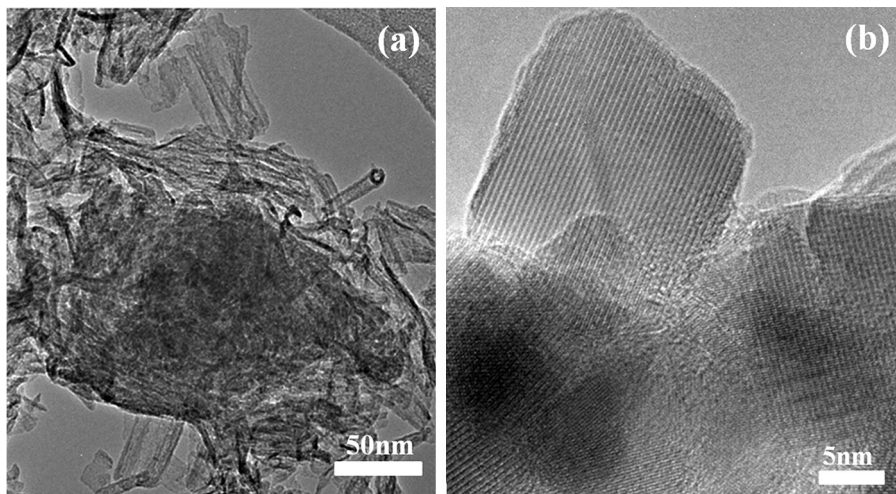


Fig. 1. TEM images of TAN sample prepared by alkali treatment.

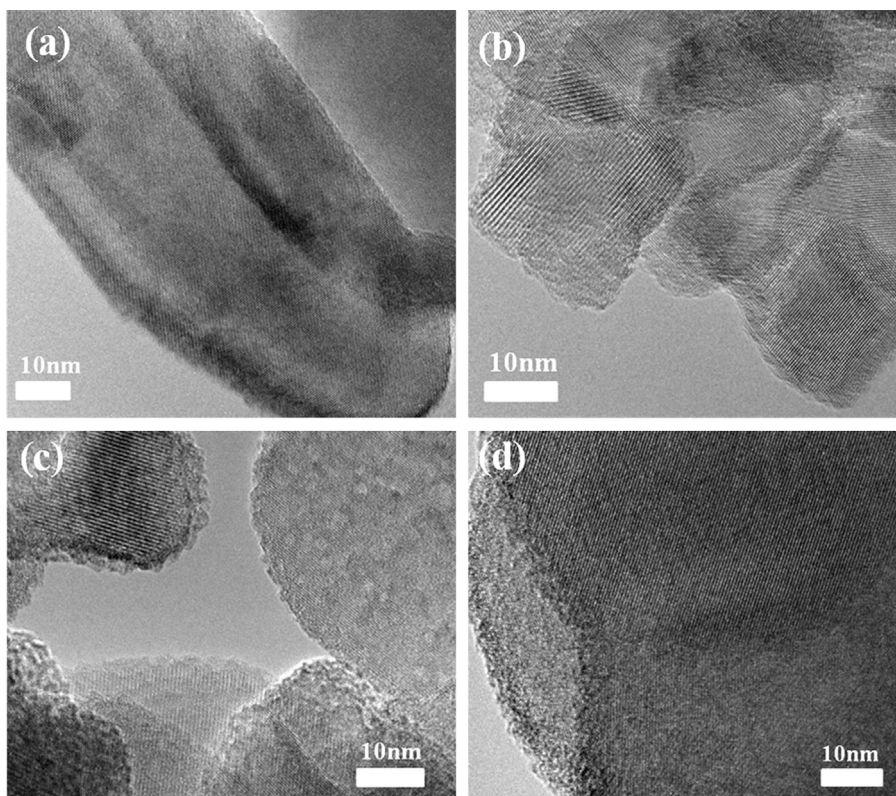


Fig. 2. TEM images of black TAN samples treated by hydrogen plasma, (a) TAN-350, (b) TAN-Cr-350, (c) TAN-500, and (d) TAN-Cr-500.

advantages of simple device and few restrictions. During the treatment process, the obtained TAN sample was loaded in a corundum boat under the filament. The temperature of the filament was maintained at 2000 °C, and the samples were treated for 3 h at 350 and 500 °C, obtained TAN-350 and TAN-500, respectively. In order to verify the effect of Cr, some Cr fragments (99.95%, Yingxin Ltd., Co., Shanghai) were mixed in the TAN sample during the treatment process, and obtained TAN-Cr-350 and TAN-Cr-500, respectively.

2.2. Characterization

High resolution transmission electron microscopy (HR-TEM, Tecnai-G2-F30) was used to examine the microstructure of the samples. Raman spectrum was recorded at room temperature using JY-HR800 Raman spectrometer, X-ray diffraction (XRD) was carried out using an X-ray diffraction analyzer (PANalytical X'Pert) and electron spin resonance (ESR) spectra were obtained at room temperature with micro frequency at 8982 MHz, which were used to characterize the phase and components of the samples. UV–vis diffuse reflectance spectra (DRS) were obtained using T1901 spectrometer by using BaSO₄ as a reference.

2.3. Photocatalytic studies

The photocatalytic activities of the samples were evaluated by monitoring the decomposition of rhodamine B (RhB) in an aqueous solution under simulated solar light irradiation (HSX-F/UV300, 50W). The photocatalyst (10 mg) was dispersed in 50 mL RhB

aqueous solution (2 mg/L) in a crystalline dish. The suspension was stirred in the dark for 1 h to establish the adsorption–desorption equilibrium. Then the light was turned on to start the photocatalytic reaction, followed by 4 mL solution was taken at a certain time interval (10 min). RhB adsorption spectra were obtained on the UV–vis spectrophotometer after removing the photocatalysts and the degradation efficiency was measured by C/C_0 (C and C_0 are the peak intensity at 554 nm of the absorption spectra measured at different time t and at the beginning, respectively).

3. Results and discussion

3.1. Morphology and components

TEM images of the obtained TAN sample demonstrate that titanate nanotubes (or nanorods) and nanosheets are formed when the titania particles are treated by concentrated NaOH solution at high temperature, as shown in Fig. 1a. Though some nanotubes (or nanorods) and nanosheets are produced, the dominant of the obtained sample is still nanoparticles (Fig. 1b). This may be caused by the short treatment time, compared with 48 h others used [31]. In order to observe the microstructure, the obtained samples treated with hydrogen plasma (see ESI, Fig. S1) were examined by HR-TEM. Compared to pristine TAN nanoparticles with clear lattice fringes shown in Fig. 1b, the black titanate nanoparticles have a disorder amorphous layer surrounding a crystalline core to form an amorphous shell/crystalline core structure (Fig. 2). Fig. 2a and c are HR-TEM images of TAN treated by hydrogen plasma at 350

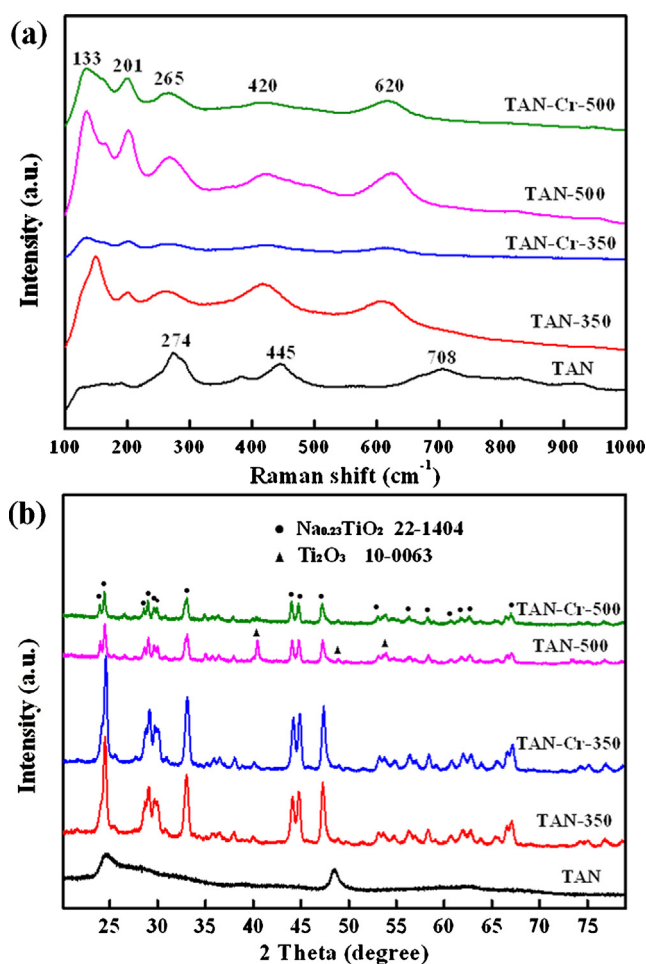


Fig. 3. Raman spectra and XRD patterns of the obtained samples.

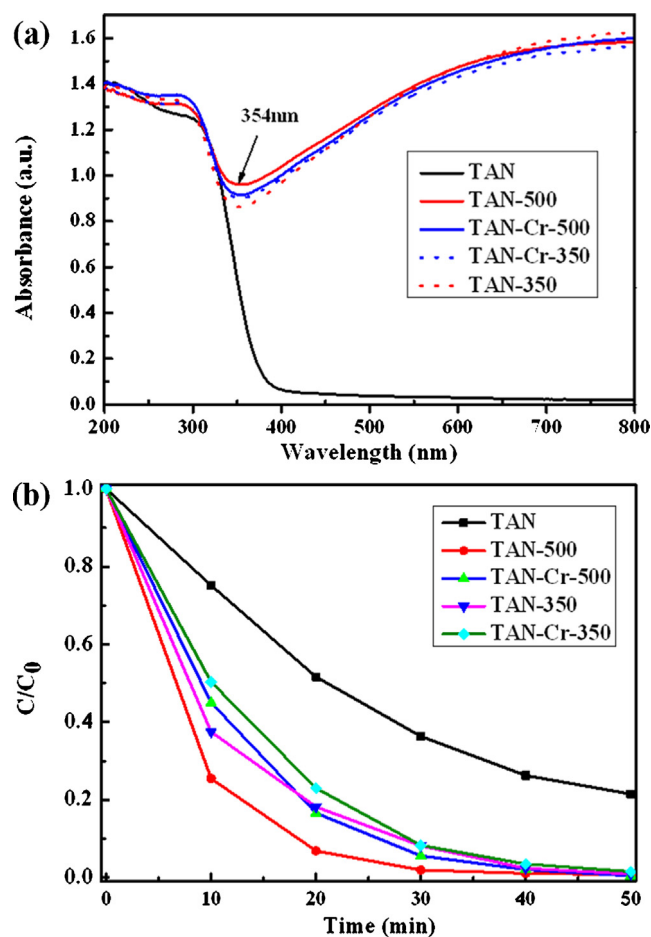


Fig. 4. (a) Diffuse reflectance spectra of our TAN samples, and (b) photocatalytic degradation of rhodamine B with the obtained samples as photocatalysts under solar light.

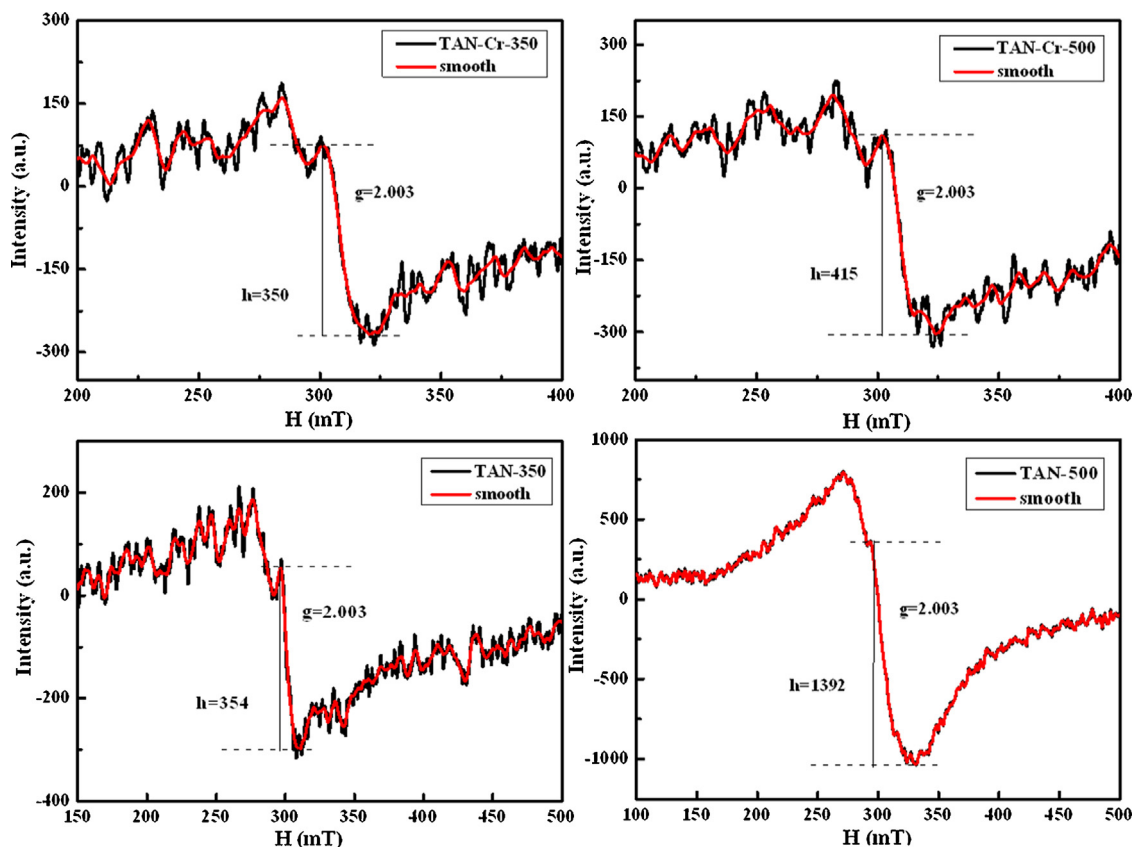


Fig. 5. ESR spectra of the samples after hydrogen plasma treatment.

and 500 °C, respectively. Fig. 2b and d are the images of samples treated at 350 and 500 °C when Cr fragments were added. Fig. 2a shows the image of a split titanate nanotube and the disorder layer cannot be observed obviously, but a thin disorder layer (~1 nm) can be observed from Fig. 2b. HRTEM images (Fig. 2c and d) show that the surface of TiO₂ nanoparticles became disordered after the treatment of hydrogen plasma at 500 °C, and the disordered outer layer is about 3–4 nm in thickness. Structural properties of black TAN samples were further examined by measuring the Raman scattering (Fig. 3a). For original TAN, three peaks at 274, 445 and 708 cm⁻¹ can be observed, which may be corresponding to the broadening and frequency shift of three rutile modes (238, 447 and 684 cm⁻¹). Compared with the six Raman active modes (3Eg + 2B_{1g} + A_{1g}) of anatase phase and two modes (Eg + A_{1g}) of rutile phase, the peaks of the treated TAN samples at 133, 201, 265, 420 and 620 cm⁻¹ are able to find good counterparts, which broadening and shift caused by defects and impurities [36]. From the broadening and shift of these peaks, it is obvious that the crystalline of the samples are changed compared with the original P25 particles. And the change of crystalline can also be confirmed from the XRD patterns of the samples (Fig. 3b). The XRD patterns demonstrate that a small amount of sodium ions (Na⁺) are embedded in the lattice of TiO₂ and form Na_{0.23}TiO₂ (JCPDS No. 22-1404) after alkali treatment, and oxygen vacancies are produced after hydrogen plasma treatment (Ti₂O₃, JCPDS No.10-0063). Because the amount of the chromium ions (Cr³⁺) is small (EDX, Fig. S2 in ESI), the existence of Cr element cannot be observed from the XRD patterns.

3.2. Photocatalytic degradation of RhB and its mechanism analysis

Fig. 4a displays the DRS of the original TAN and treated TAN samples. For all samples, the absorption at wavelengths shorter

than 400 nm can be attributed to the intrinsic bandgap absorption of TiO₂. Compared with original TAN, the samples treated by hydrogen plasma possess a significant absorption in the visible and near infrared region. But the sample annealed 500 °C with Cr³⁺ has weaker absorption than the sample without Cr³⁺. Because of the difference of solar absorbance, the photocatalytic activity of the samples is also different. The data in Fig. 4b demonstrate the increased photocatalytic activity of the treated TAN samples compared with the original TAN, and the TAN-500 has the highest photocatalytic activity in all the samples. Fig. 5 shows the ESR spectra of the plasma-treated TAN samples, which are widely-used to examine unpaired spins. For all the samples, a sharp signal appeared at $g=2.003$, which was related to the oxygen vacancy with a trapped electron [37]. And from the intensity of the signals, we can speculate that TAN-500 has more oxygen vacancies than others, which may be the major reason of its high photocatalytic activity [38].

The efforts of the plasma treatment for the samples are discussed as follows. Hydrogen plasma process offers high-energy species such as electron, atoms and radicals, which improve thermodynamics and kinetics over conventional processing. It is the key why our samples are much easier be converted in black than the H₂-annealing sample [20]. The surface layer of the TiO₂ nanoparticles is reduced by the hydrogen ions with high activity and a lot of oxygen vacancies (Vo) and Ti–H bonds are produced, then a disorder layer is formed. Owing to the appearance of the disorder layer, a smaller sized crystalline core is obtained and the intrinsic bandgap is widen (about 3.5 eV), which is the reason that the samples after treatment have an absorption valley at $\lambda=354$ nm. But the bandgap of the samples is narrowed to about 2.8 eV estimated from the DSR. In order to further understand our black TAN samples, the energy band and structure diagram scheme are schematized in Fig. 6. Wang et al. [20] found that the disorder shell of TiO₂ loses

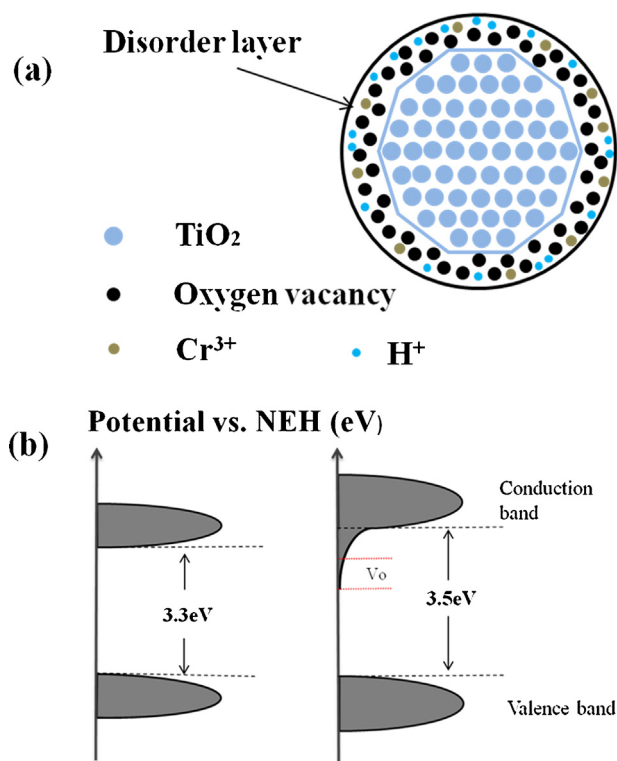


Fig. 6. Schematic of the structure and DOS for the black TAN sample.

lattice periodicity and breaks the octahedral symmetry of TiO_6 , and a tail of the conduction band (CB) is formed which can narrow the band gap. From the calculated total and projected density of states (DOS), the primary effect of surface defects and reconstruction in TiO_2 nanocrystals is to produce strong band tailing near the conduction band edge. And hydrogen atoms introduce localized states below the CB minimum of TiO_2 nanoparticles. Therefore, the electronic transitions from both tailed CB, V_o localized states and mid-gap electronic states to CB are responsible for the visible and near infrared light absorption in our samples. And V_o and Ti–H bonds are the dominant impact to make the sample display black coloration and have high photocatalytic activity. When Cr was introduced into the TiO_2 nanoparticles, the photocatalytic activity is reduced. The reason is that Cr ions in the disorder layer can reduce the content of oxygen vacancy (ESR spectra) and weaken the absorption of light (DRS).

4. Conclusions

In summary, we have shown that our black TAN samples exhibit unique light absorption property because a disorder layer is formed after hydrogen plasma treatment, which may be caused by numerous oxygen vacancies and Ti–H bonds. The bandgap narrowing is dictated by the synergistic presence of V_o and Ti–H bonds. And the Cr ions have the opposite effect *via* reduce the content of V_o , which is confirmed that it is unnecessary to introduce Cr into the preparation of black TiO_2 . The findings of this work also provide new insights for developing nanostructures tailored for solar conversion device and other applications via controlled bandgap engineering.

Acknowledgements

This project was supported by the National Natural Science Foundation of China (no. 61176058), Natural Science Foundation of Gansu Province (no. 1107RJYA280) and Program for Changjiang

Scholars and Innovative Research Team in University (Grant no. IRT1251).

Appendix A. Supplementary data

Supplementary material related to this article can be found, in the online version, at <http://dx.doi.org/10.1016/j.apcatb.2013.11.015>.

References

- [1] R. Leary, A. Westwood, Carbon 49 (2011) 741–772.
- [2] B. Tryba, T. Tsumura, M. Janus, A.W. Morawski, M. Inagaki, Applied Catalysis B: Environmental 50 (2004) 177–783.
- [3] J.H. Im, S.J. Yang, C.H. Yun, C.R. Park, Nanotechnology 23 (2012) 1–10, 035604.
- [4] J. Zhang, Q. Xu, Z.C. Feng, M.J. Li, C. Li, Angewandte Chemie International Edition 47 (2008) 1766–1769.
- [5] E.J.W. Crossland, N. Noel, V. Sivaram, T. Leijtens, J.A. Alexander-Webber, H.J. Snaith, Nature 495 (2013) 215–219.
- [6] Q.I. Rahman, M. Ahmad, S.K. Misra, M. Lohani, Materials Letters 91 (2013) 170–174.
- [7] C. Lin, Y. Song, L.X. Cao, S.W. Chen, Nanoscale 5 (2013) 4986–4992.
- [8] W. Wang, C.H. Lu, Y.R. Ni, J.B. Song, M.X. Su, Z.Z. Xu, Catalysis Communications 22 (2012) 19–23.
- [9] L.Q. Ye, K.J. Deng, F. Xu, L.H. Tian, T.Y. Peng, L. Zan, Physical Chemistry Chemical Physics 14 (2012) 82–85.
- [10] T. Ihara, M. Miyoshi, M. Ando, S. Sugihara, Y. Iriyama, Journal of Materials Science 36 (2001) 4201–4207.
- [11] G.M. Wang, H.Y. Wang, Y.C. Ling, Y.C. Tang, X.Y. Yang, R.C. Fitzmorris, C.C. Wang, J.Z. Zhang, Y. Li, Nano Letters 11 (2011) 3026–3033.
- [12] W.Q. Han, L.J. Wu, Y.M. Zhu, K. Watanabe, T. Taniguchi, Applied Physics Letters 93 (2008) 223103 1–223103 3.
- [13] Z.L. He, W.X. Que, H.X. Xie, J. Chen, Y. Yuan, P. Sun, Journal of American Ceramic Society 95 (2012) 3941–3946.
- [14] H.W. Bai, Z.Y. Liu, D.D. Sun, Journal of Materials Chemistry 22 (2012) 18801–18807.
- [15] D.H. Wang, L. Jia, X.L. Wu, L.Q. Lu, A.W. Xu, Nanoscale 4 (2012) 576–584.
- [16] C.X. Feng, Y. Wang, Z.S. Jin, J.W. Zhang, S.L. Zhang, Z.S. Wu, Z.J. Zhang, New Journal of Chemistry 32 (2008) 1038–1047.
- [17] K. Sridharan, T.J. Park, Applied Catalysis B: Environmental 134/135 (2013) 174–184.
- [18] W. Choi, A. Termin, M.R. Hoffmann, The Journal of Physical Chemistry 98 (1994) 13669–13679.
- [19] X.B. Chen, L. Liu, P.Y. Yu, S.S. Mao, Science 331 (2011) 746–750.
- [20] Z. Wang, C.Y. Yang, T.Q. Lin, H. Yin, P. Chen, D.Y. Wan, F.F. Xu, F.Q. Huang, J.H. Lin, X.M. Xie, M.H. Jiang, Advanced Functional Materials 23 (2013) 5444–5450.
- [21] Z.K. Zheng, B.B. Huang, J.B. Lu, Z.Y. Wang, X.Y. Qin, X.Y. Zhang, Y. Dai, M.H. Whangbo, Chemical Communications 48 (2012) 5733–5735.
- [22] S. Hoang, S.P. Berglund, N.T. Hahn, A.J. Bard, C.B. Mullins, Journal of American Chemical Society 134 (2012) 3659–3662.
- [23] Z.X. Pei, L.Y. Ding, H. Lin, S.X. Weng, Z.Y. Zheng, Y.D. Hou, P. Liu, Journal of Materials Chemistry A 1 (2013) 10099–10102.
- [24] T. Xia, X.B. Chen, Journal of Materials Chemistry A 1 (2013) 2983–2989.
- [25] L. Liu, P.Y. Yu, X.B. Chen, S.S. Mao, D.Z. Shen, Physical Review Letters 111 (2013) 1–5, 065505.
- [26] Z. Wang, C.Y. Yang, T.Q. Lin, H. Yin, P. Chen, D.Y. Wan, F.F. Xu, F.Q. Huang, J.H. Lin, X.M. Xie, M.H. Jiang, Energy Environmental Science 6 (2013) 3007–3014.
- [27] X.B. Chen, L. Liu, Z. Liu, M.A. Marcus, W.C. Wang, N.A. Oyler, M.E. Grass, B.H. Mao, P.A. Glans, P.Y. Yu, J.H. Guo, S.S. Mao, Scientific Reports 3 (2013) 1510 1–1510 7.
- [28] X.D. Jiang, Y.P. Zhang, J. Jiang, Y.S. Rong, Y.C. Wang, Y.C. Wu, C.X. Pan, The Journal of Physical Chemistry C 116 (2012) 22619–22624.
- [29] W. Wang, Y.R. Ni, C.H. Lu, Z.Z. Xu, RSC Advances 2 (2012) 8286–8288.
- [30] J.B. Lu, Y. Dai, H. Jin, B.B. Huang, Physical Chemistry Chemical Physics 13 (2011) 18063–18068.
- [31] A. Danon, K. Bhattacharyya, B.K. Vijayan, J.L. Lu, D.J. Sauter, K.A. Gray, P.C. Stair, E. Weitz, ACS Catalysis 2 (2012) 45–49.
- [32] T. Kasuga, M. Hiramatsu, A. Hoson, T. Sekino, K. Niihara, Advanced Materials 11 (1999) 1307–1311.
- [33] T. Kasuga, M. Hiramatsu, A. Hoson, T. Sekino, K. Niihara, Langmuir 14 (1998) 3160–3163.
- [34] F. Teng, J.T. Wang, X.Y. An, B.A. Lu, Y.R. Su, C.S. Gong, P. Zhang, Z.X. Zhang, E.Q. Xie, RSC Advances 2 (2012) 7403–7405.
- [35] F. Teng, P. Zhang, G.Z. Zhang, C.S. Gong, C.T. Gao, X.W. Fu, J.T. Wang, Z.X. Zhang, X.J. Pan, E.Q. Xie, Materials Letters 115 (2014) 9–12.
- [36] V. Swamy, Physical Review B 77 (2008) 195414 1–195414 4.
- [37] I. Nakamura, N. Negishi, S. Kutsuna, T. Ihara, S. Sugihara, K. Takeuchi, Journal of Molecular Catalysis A: Chemical 161 (2000) 205–212.
- [38] A. Naldoni, M. Allietta, S. Santangelo, M. Marelli, F. Fabbri, S. Cappelli, C.L. Bianchi, R. Psaro, V.D. Santo, Journal of American Chemical Society 134 (2012) 7600–7603.